Journal of Physics: Condensed Matter

Fermi surface map of large-scale single-orientation graphene on SiO_2

OPEN ACCESS
IOP Publishing
Journal of Physics: Condensed Matter
J. Phys.: Condens. Matter **29** (2017) 475001 (8pp)
https://doi.org/10.1088/1361-648X/aa8f27

Fermi surface map of large-scale single-orientation graphene on SiO_2

E Miniussi[1], C Bernard[1], H Y Cun[1,2], B Probst[3], D Leuenberger[1], G Mette[1,4], W-D Zabka[1], M Weinl[5], M Haluska[6], M Schreck[5], J Osterwalder[1] and T Greber[1]

[1] Physik-Institut, Universität Zürich, Winterthurerstrasse 190, CH-8057 Zürich, Switzerland
[2] Laboratory of Nanoscale Biology, Institute of Bioengineering, School of Engineering, EPFL, 1015 CH-Lausanne, Switzerland
[3] Department of Chemistry, University of Zürich, Winterthurerstrasse 190, CH-8057 Zürich, Switzerland
[4] Philipps-Universität Marburg Fachbereich Physik, D-35032 Marburg, Germany
[5] Universität Augsburg, Institut für Physik, D-86135 Augsburg, Germany
[6] Micro- and Nanosystems, DMAVT ETH Zürich, Tannenstrasse 3, CH-8092 Zürich, Switzerland

E-mail: greber@physik.uzh.ch

Received 6 June 2017, revised 29 August 2017
Accepted for publication 26 September 2017
Published 31 October 2017

Abstract

Large scale tetraoctylammonium-assisted electrochemical transfer of graphene grown on single-crystalline Ir(1 1 1) films by chemical vapour deposition is reported. The transferred samples are characterized in air with optical microscopy, Raman spectroscopy and four point transport measurements, providing the sheet resistance and the Hall carrier concentration. In vacuum we apply low energy electron diffraction and photoelectron spectroscopy that indicate transferred large-scale single orientation graphene. Angular resolved photoemission reveals a Fermi surface and a Dirac point energy which are consistent with charge neutral graphene.

Keywords: epitaxial graphene, Ir (1 1 1) films, Raman spectroscopy, Fermi surface mapping, graphene transfer

Supplementary material for this article is available online

(Some figures may appear in colour only in the online journal)

1. Introduction

Ultrathin two dimensional (2D) materials are expected to revolutionize materials science and technology [1–3]. The production of 2D systems like graphene (*g*) relies on exfoliation from pristine bulk samples [4, 5] or from substrates on which the materials have been synthesized [6]. While dry transfer is promising on small scales [7], so far, wet transfer methods produce larger scale graphenes that are e.g. needed in conventional photoemission experiments.

Photoemission from graphene [8–12] yields direct insight into the electronic structure and the measurement of relevant quantities like the Dirac energy and the Fermi velocity. The experiments on freestanding [13] and/or transferred [14, 15] samples pose more challenges due to the difficulty of producing large-scale films, and, up to date, most results found in literature are for micrometer-sized samples [8, 16, 17].

Here, we report on the growth of graphene on Ir(1 1 1) by chemical vapour deposition (CVD) [18] and subsequent exfoliation of square centimeters of single-layer graphene with single-orientation from recyclable substrates. CVD is an established method for the synthesis of epitaxial graphene on close-packed surfaces of many transition metals. Twin-free, single-crystalline metal films of the Pt group grown on YSZ-buffered Si(1 1 1) substrates are an alternative to expensive

and size-limited bulk single-crystals [19]. We are able to synthesise single-domain sp^2 hybridized films on 150 nm-thick Ir(1 1 1)/YSZ/Si(1 1 1) 4-inch wafers [20]. After growth the graphene has to be delaminated from the substrate. The electrochemical delamination (known as the bubbling method) [21] performs well for graphene on copper [22, 23], but until recently only limited transfer rates could be achieved for graphene on Ir single-crystals. For exfoliation of graphene grown on stepped Ir(3 3 2), Rakić *et al* introduced a further step and first intercalated graphene with Cs in order to enable the subsequent electrochemical delamination of the carbon film [24]. In the present paper the recently introduced two step wet transfer protocol for graphene on iridium of Koefoed *et al* is applied [25]. After delamination, the material was transferred onto insulating SiO_2/Si(0 0 1)substrates. On these samples we measured with photoemission Fermi surface maps, which confirm that the transferred material has single-orientation across the whole sample area and which indicate charge neutral graphene.

2. Experimental

2.1. Sample preparation

The untwinned (1 1 1)-oriented, 150 nm-thick, Ir(1 1 1)/ YSZ/ Si(1 1 1) substrates were cleaned by repeated Ar^+ sputtering ($E_{kin} = 0.8$ keV) and annealing cycles up to 1170 K, followed by an oxygen treatment ($p_{max}(O_2) = 1 \times 10^{-7}$ mbar; $500 < T < 870$ K) and a final flash annealing up to 1220 K. Single-layer graphene was synthesized by ethylene (C_2H_4) CVD at $T = 1140$ K in UHV conditions according to a well-established procedure [26] (figure 1(b-I)). Low energy electron diffraction (LEED) shows a sharp moiré pattern around the first-order spots of the substrate with low background intensity, thus confirming long-range order of the film.

2.2. TOA-assisted electrochemical delamination

Following the method developed by Koefoed *et al* [25], the *g*/Ir samples were treated with a 0.1 M tetraoctylammonium-bromide (TOABr, figure 1(a))/acetonitrile solution prior to the electrochemical delamination [23, 27] of the graphene films, as shown in figure 1(b-II).

A number of studies [25, 28, 29] show larger transfer yields achieved when using the TOA-assisted method. Tetraalkylammonium compounds are supposed to weaken the van der Waals interactions of sp^2 materials with the underlying metal [25, 30], thus facilitating the subsequent delamination step.

In order to promote the migration of TOA^+ ions to the *g*/Ir interface, a bias voltage of -1.9 V is first applied between the working electrode and the Ag reference electrode for 10 min. Shorter application times of the negative bias result in an incomplete detachment of the graphene layer (only the edge regions are efficiently transferred, see supplementary figure 1 (stacks.iop.org/JPhysCM/29/475001/mmedia)). To prevent reaction of the negatively charged graphene with the

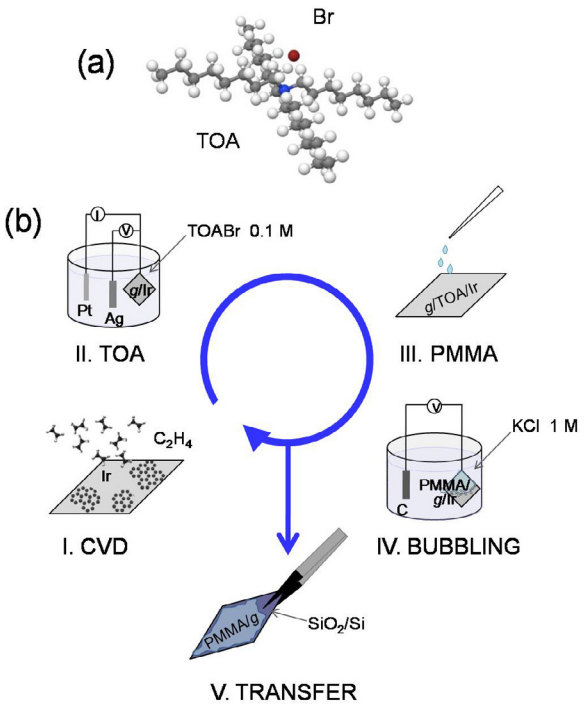

Figure 1. (a) Atomic model of the TOABr ($C_{32}H_{68}BrN$) molecule. (b) Schematics of the experimental procedure: (I) graphene synthesis on the Ir substrate via high-temperature C_2H_4 CVD; (II) electrochemical TOA treatment; (III) PMMA spin-coating; (IV) electrochemical graphene delamination from the substrate in a KCl electrolyte solution; (V) transfer onto a SiO_2/Si substrate.

polymethylmetacrylate (PMMA) layer [25], the *g*/Ir electrode is then discharged for 20 s at a potential of -0.2 V.

The TOA-treated *g*/Ir sample is subsequently rinsed with acetonitrile and dried in N_2 atmosphere, spin-coated with a 4wt.% PMMA 495 K solution (figure 1(b-III)) and dried overnight in ambient air at room temperature. The electrochemical delamination is performed with the bubbling method [21–23], using a two-electrode setup consisting of the *g*/Ir sample as a working electrode and a graphite rod as counter electrode immersed in a 1 M KCl aqueous solution (figure 1(b-IV)). The *g*/Ir electrode is cathodically polarized at about -5 V and gradually immersed into the solution. H_2 bubbles form at the *g*/Ir interface due to water reduction ($2H_2O(l) + 2e^- \longrightarrow H_2(g) + 2OH^-(aq)$) and induce the detachment of the graphene/PMMA film from the substrate, starting at the edges and subsequently extending to other regions of the film as the electrolyte solution permeates the *g*/Ir interface. The delaminated *g*/PMMA film is rinsed for half an hour in a flow of ultrapure water (provided by a Milli-Q Advantage A10 water purification system) and then deposited on a clean 10×10 mm^2 SiO_2/Si substrate. The PMMA/*g*/SiO_2 sample is heated overnight at 400 K. Finally, the PMMA is removed via a sequence of acetone/ethanol baths at 370 K and the *g*/SiO_2 sample is annealed in air at 400 K for about 30 min.

2.3. Sample characterization

Optical images were acquired using a Leica DMV2500 stereomicroscope.

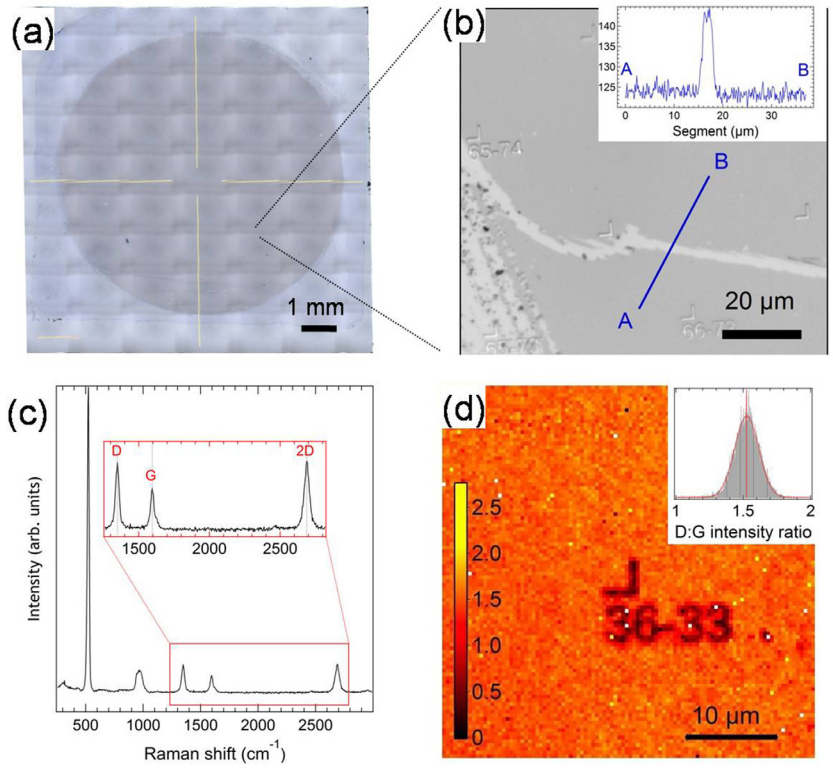

Figure 2. (a) Optical microscopy image of a $g/SiO_2/Si$ sample with gold markers after TOA-assisted electrochemical delamination from the Ir substrate. The image was obtained by stitching multiple optical images with 150× magnification. The round shape of the graphene-covered area is due to the presence of a fixation ring mounted on the Ir substrate during graphene growth. (b) Zoom-in of (a), with a 2000× magnification and applying a 550 nm filter. The inset displays a line profile of the optical contrast between graphene-covered regions (darker areas) and bare substrate (lighter areas). Oxide thickness 100 nm. (c) Representative Raman spectrum (excitation with $\lambda = 532$ nm) of the $g/SiO_2/Si$ sample (D:G ratio = 1.5); the inset is a zoom-in of the graphene-fingerprint region with the D-, the G- and the 2D-band. (d) Map of the Raman D:G integrated peak ratio over an area of 40×40 μm (36–33 is a gold marker used to localize the same spot in different microscopes). The inset shows the D:G histogram, where the Gaussian fit indicates an average D:G ratio of 1.52 ± 0.27.

Raman measurements were performed with a Witec confocal Raman microscope with a 532 nm laser wavelength and a diffraction-limited lateral resolution of 340 nm (the full width of half maximum (FWHM) of the laser spot using a 100× objective (NA = 0.8) is 0.3 μm). Raman maps were collected using a spatial step size of 400 nm, a grating with 600 lines mm^{-1}, laser power of 0.5 mW, and an integration time of 4.5 s per spectrum. The D, G and 2D-bands were fitted with single-peak Voigt functions (resulting from the convolution of a Gaussian and a Lorentzian profile), using a straight line to describe the local background.

Secondary electron microscopy (SEM) images (supplementary figure 6) were acquired using a Zeiss Supra 50 VP field emission scanning electron microscope. Measurements were performed using the inlens detector and primary electron energies between 2 and 2.5 keV.

X-ray photoelectron spectroscopy (XPS) and angular resolved photoelectron spectroscopy (ARPES) were acquired using Mg Kα and He IIα radiation [31]. The total He IIα photoelectron current from the g/SiO_2 sample was 7.6 nA, almost twice as large as the value (3.9 nA) measured for a reference Ag polycrystal under otherwise identical conditions. This translates, with a photon spot size of 3.2 mm^2 and a quantum efficiency of about 6.5% for Ag [32], into a flux density of 1.2×10^{11} photons/(s mm^2).

3. Results

3.1. Microscopy and Raman characterisation

The optical contrast between graphene and the substrate depends on the SiO_2 layer thickness and on the wavelength of the detection light [33–35]. It arises from the interference between the light reflected at the graphene surface or the bare SiO_2 and at the interface between oxide and silicon [36]. An appropriate choice of the SiO_2 layer thickness and excitation wavelength thus enables to efficiently detect the presence and distribution of graphene. In the present work, SiO_2/Si wafer samples with oxide thicknesses between 74 and 100 nm were used and for 100 nm an optical contrast of $13 \pm 1\%$ at 550 nm was measured using a standard green filter (see figure 2(b)).

A comparison with optical microscopy data for SiO_2-supported multilayer graphene transferred from Cu foil (supplementary figure 2) confirms the absence of multi-layer graphene.

Graphene is most often characterized by two main bands in the Raman spectrum: the G-band (at about 1580 cm^{-1}), which is a first-order in-plane vibrational mode, and the 2D-band (at about 2690 cm^{-1}), a second-order in-plane mode. The Raman shift of this mode is approximately double that of the in-plane breathing mode, D (~1350 cm^{-1}, depending on the excitation wavelength) [37]. The D-band originates from defect-induced intervalley phonon scattering [38–41], and makes this

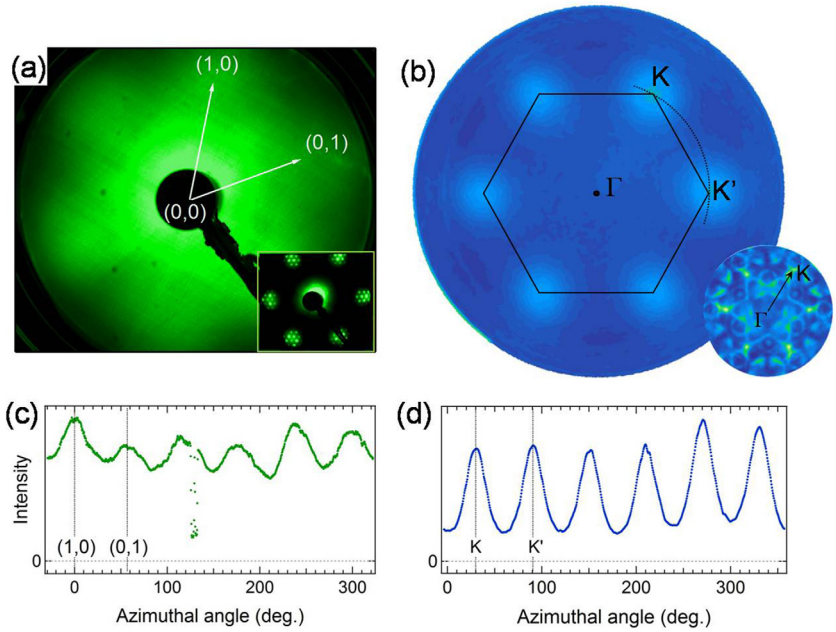

Figure 3. (a) LEED pattern of a transferred g/SiO_2 sample at 70 eV. The reciprocal lattice vectors are superimposed; in the inset the LEED pattern of a g/Ir preparation is shown. (b) Fermi surface of the transferred graphene sample in (a) acquired with He IIα radiation. The first Brillouin zone of graphene is superimposed. In the inset the Fermi surface of g/Ir is shown. (c)–(d) Azimuthal line profile across the high symmetry points (c) of the LEED pattern in (a) and (d) of the Fermi surface map in (b) (on the azimuthal cut across $\bar{\mathrm{K}}\bar{\mathrm{K}}$ 1 degree corresponds to 2.97×10^{-2} Å^{-1}). Note the higher contrast achieved in photoemission (d) with respect to LEED (c).

spectroscopy one of the most sensitive techniques to characterize disorder in sp^2 carbon systems.

A representative Raman spectrum of $g/SiO_2/Si$ is shown in figure 2(c). The three bands yielding the fingerprint of graphene [40] can be clearly identified: the D peak at 1350 cm^{-1}, the G peak at 1600 cm^{-1}, and the 2D peak at 2695 cm^{-1}. The observed blue-shift of the G-band could be ascribed to doping by charge impurities present on the SiO_2/Si substrate [42, 43]. It has been shown that the G mode frequency increases as a function of both electron and hole doping [44, 45]. Ni *et al* reported a large blue shift of the G-band (up to 15 cm^{-1}) for single layer graphene after SiO_2 deposition on the graphene surface followed by annealing in air and explained the blue shift in terms of compressive stress [46].

The analysis of Raman data enables extracting quantitative information on the sample, such as the number of graphene layers and the local defect density [38, 41]. The shape of the 2D peak (with an average Voigt FWHM of 21 cm^{-1}) confirms the single-layer thickness of the graphene film, since any additional layer would result in a larger broadening of the 2D-band [41, 47]. As explained in earlier works [48, 49], the D:G ratio can be used to estimate the defect density. Although the LEED data of most g/Ir preparations indicate high quality graphene films (an example is shown in figure 3(a)), the Raman spectra of the g/Ir (supplementary figure 3) and the transferred samples exhibit a significantly stronger D-band contribution than typically observed in samples transferred from polycrystalline Cu (see supplementary figure 4). A 40×40 μm^{-2} Raman map of the D:G intensity ratio is shown in figure 2(d). The presence of gold markers in the middle of the scanned area induces an alteration of the spectra, resulting in a fictitiously low D:G ratio; those points were therefore excluded from the analysis. Figure 2(d) shows the D:G intensity ratio histogram, with a peak at 1.52 ± 0.27. Assuming point defects and using the conversion equation and parameter values reported in [50], this translates into a defect density of $1.30 \pm 0.28 \times 10^{13}$ cm^{-2}, meaning three to four structural defects (for example missing C atoms) every 1000 C atoms. Experiments on commercial g/Cu samples (provided by the Institute of Electronic Materials Technology in Warsaw), in which the TOA-assisted method was compared to the standard delamination procedure, showed no effect of the TOA-pretreatment on the Raman spectra (supplementary figure 5).

3.2. Transport properties of g/SiO_2

In order to gain insight into the macroscopic charge transport properties of the graphene transferred from Ir(1 1 1) onto SiO_2, the sheet resistance and the Hall carrier sheet density were determined with the van der Pauw four point probe method [51–53] (see supplementary section 9).

More than a week after transfer the set of four different 2×2 mm^2 samples displayed sheet resistances of 2.9 ± 1.3 kΩ and a Hall carrier concentration of $(2 \pm 5)10^{13}$ cm^{-2}, where we found n-type as well as p-type conductivity. The best room temperature carrier mobility we found was 400 cm^2 Vs^{-1}. It is low compared to literature values for suspended graphene [54–56], though in line with the defect-density indicated by Raman spectroscopy.

3.3. Atomic and electronic structure of g/SiO_2

The chemical composition of the transferred graphene samples was investigated by conventional core level photoelectron

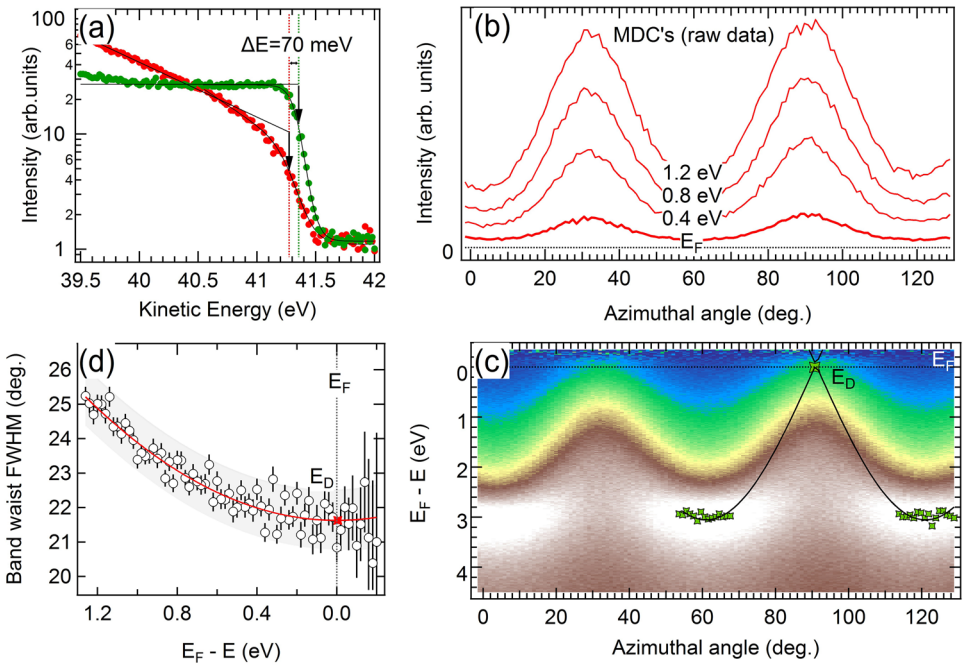

Figure 4. (a) Comparison of the Fermi edge of g/SiO_2 measured 30° from the K points (red data points) and that of polycrystalline Ag (green data points), on the kinetic energy scale of the analyzer, on a logarithmic scale. The solid black lines are Fermi functions multiplied by an exponential function (g/SiO_2) or a constant factor (Ag) on top of a constant background. The arrows indicate the factor $1/2$ by which the intensity drops at the Fermi step. With respect to Ag, the Fermi level of g/SiO_2 appears shifted by 70 meV to lower kinetic energies, which indicates charging of g/SiO_2. The effective temperatures T_{eff} are 600 K for polycrystalline Ag and 900 K for g/SiO_2. (b) Momentum distribution curves on a polar emission angle of 34° (from the normal emission) as a function of azimuthal angle at 0, 0.4, 0.8, and 1.2 eV binding energy ($E_F - E$). (c) π-band dispersion across the Dirac cone features in the Fermi surface map of figure 3(b). The data have been background-subtracted and normalized with the effective Fermi function. A tight binding model fit using the experimentally determined Dirac point and the local π-band intensity maxima $> 15°$ away from the K points is superimposed to the data. (d) π-band width as a function of binding energy. The individual I(ϕ) curves in (b) have been fitted with two Gaussians centered at K and K′ and the corresponding average FWHM is shown. The red line is a parabolic fit with a minimum near the Fermi level (-2 ± 90 meV binding energy). The grey-shaded area is the 2σ prediction band.

spectroscopy. Prior to the *ex situ* measurements, a mild annealing at 670 K for about 40 min was performed in order to desorb contaminants. The quantitative evaluation of the data allows to estimate the graphene transfer rate from Ir onto SiO_2. In supplementary figure 7 the C 1*s* and Ir 4*d* core level spectra prior to and after transfer are compared. The same XPS analysis was applied to several sample preparations, resulting in consistently high transfer rates between 70 and 95%.

Insight into the crystallinity of the transferred g/SiO_2 samples was gained with low energy electron diffraction and angular resolved photoelectron spectroscopy, where Fermi surface (FS) mapping is particularly useful. The LEED pattern of a SiO_2-supported sample is shown in figure 3(a): The six-fold symmetry with diffraction maxima centered at the graphene reciprocal lattice sites indicates a preferential orientation of the transferred graphene film on the amorphous SiO_2 substrate. Apparently the single-orientation that is obtained during the growth on the single crystalline Ir(1 1 1) substrates survives the transfer. The LEED pattern of as grown pristine g/Ir is shown for comparison in the inset of figure 3(a). Besides the sharp principal spots, it also displays the moiré superstructure of g/Ir(1 1 1) [18] that does not survive the transfer.

Figure 3(b) shows the Fermi surface of a g/SiO_2 sample acquired with He IIα ($h\nu = 40.8$ eV) radiation. The maxima centered at six symmetric points 1.72 ± 0.02 Å^{-1} away from normal emission (Γ point) coincide with the locations of the K-points of the graphene Brillouin zone where the Dirac cones are expected. This confirms the preserved azimuthal orientation of the electronic band structure of the graphene layer on SiO_2. The quantitative comparison between the LEED pattern and the FS map in figures 3(c) and (d), respectively, demonstrates that the photoemission experiment produces a significantly higher contrast, since photoemission at the Fermi energy selectively probes the π-electrons of graphene at the K-points of the Brillouin zone, while the electrons in the LEED experiment have a scattering path twice as long and are scattered by the potential produced by all electrons. The FS of *g*/Ir before transfer, in which the six Dirac cone features are sharper, is shown for comparison in the inset of figure 3(b). This indicates that the transfer induces a smearing of the Dirac cones. This could be due to the non-planarity of the SiO_2 substrate, to charge 'puddles' [57–59] and/or to inhomogeneous charging by the photon beam. Charging is reflected in a spectral shift and inhomogeneity in a smearing of the Fermi level.

In figure 4(a) the Fermi edge of a g/SiO_2 sample extracted from an azimuthal scan 30° away from the K points is compared with that of an Ag reference sample on a logarithmic scale. Both spectra have been measured at room temperature and under identical analyzer and photon source settings. The smearing of the Fermi level of g/SiO_2 as compared to

Ag is reflected in the lower slope of the high energy wing above the Fermi level. The solid lines are fits to the spectra with Fermi functions multiplied by an exponential function on top of a constant background from which the Fermi level E_F and an effective temperature T_{eff} are determined. Effective temperatures T_{eff} of 900 K (g/SiO_2) and 600 K (Ag) were obtained. They reflect the sample temperature (300 K), the instrumental resolution [60] and the smearing of the Fermi level, which may occur upon charging. The Fermi level of g/SiO_2 is shifted by 70 meV with respect to that of the reference Ag polycrystal. This indicates that the charging of the g/SiO_2 sample may not be compensated by the graphene, and an effect on the charge carrier concentration or gating in the graphene film may be expected. In other photoemission work on graphene on SiO_2, 300 meV charging was reported [14] though not further explored.

To derive more quantitative information on the band structure of g/SiO_2 and to compare it with the Hall charge carrier density from the transport measurements, the Dirac points should be determined. This was achieved by measuring azimuthal ARPES scans at a fixed polar angle across the K and K′ points as indicated in figure 3(b). In figure 4(b) the momentum distribution curves (MDC's) for selected photoelectron energies are shown at a polar emission angle of 34° along the azimuthal emission angle. The complete ARPES data set is shown in figure 4(c) after background-subtraction and normalization by a Fermi function $(1/(1+\exp(E-E_F)/(k_BT_{eff})))$. The Fermi function has been fitted at azimuthal positions without direct transitions (data in figure 4(a)). The ARPES data show the π-band dispersion between adjacent K points along the arc superimposed to figure 3(b). Despite the smearing of the band structure, we can determine a Dirac energy from these data. The Dirac points lie at the locations where the π-band waist (i.e. the FWHM of the peaks in the MDC's (see figure 4(b)) is the narrowest. E_D was found from the plot of the waist width versus energy data. The waist FWHM was determined by fitting two Gaussian functions with a linear background to all azimuthal intensity cuts, and by taking the average FWHM of the two. We note that this determination does not depend on the normalization with the Fermi energy and therefore appears reliable. The π-band waist versus energy data follow a parabola with a local minimum close to the Fermi level, $E_F - E_D = -2 \pm 90$ meV (see figure 4(d)). This value compares well with the results obtained by Knox *et al* for free-standing exfoliated monolayer graphene, for which they report $E_F - E_D = 9 \pm 25$ meV [13].

To extract the Fermi velocity v_F a first-nearest neighbor tight binding (TB) function on the azimuthal cut of the measured dispersion in k-space was fitted to the data. The underlying theoretical approach is detailed in the supplementary data [61, 62]. The maxima of the energy distribution curves between K and K′ were used, along with the Dirac points, as support points for the TB fit. The fit returns a value of 2.55 ± 0.10 eV for the transfer integral γ_0, in good agreement with the literature: Bostwick *et al* [63], e.g. reported an experimental value of 2.82 eV in their ARPES characterization of single-layer graphene grown on SiC(0 0 0 1). Our result is also in line with TB simulations performed on single-layer graphene [64] and graphite [65]. Other Raman [66] and infrared spectroscopy [67] studies on bilayer graphene and graphite report values between 2.9 and 3.16 eV.

4. Discussion

The charge carrier density in graphene may be tuned via changes in the dielectric support. For example, in the Helmholtz inversion layer of a liquid drop on a graphene field effect transistor, minimal changes of the electrochemical potential yield a strong change of the gate voltage that has to be applied in order to reach the charge neutrality point [68]. In the present case we observe a 70 meV charging of the $g/SiO_2/Si$ *p*-type substrate. The sign of the Fermi level shift is the same as observed in photoemission experiments, where a significant Ohmic resistance induces a shift of the Fermi level, i.e. a net positive charge, which in turn produces an additional potential that the photoelectrons have to overcome. This positive charge must be localized close to the g/SiO_2 interface, in a region limited by the mean free path of the photoelectrons. The field generated by this charge must impose an up-shift of the Dirac energy, towards *p*-type conductivity of the graphene layer. With a photoelectron current of 7.6 nA, we get a resistance of 9 MΩ and, considering the photon spot size of 3.2 mm^2, the average charging of 70 meV translates into a charge density of 5×10^5 e cm^{-2}. The Fermi level shift decreases towards the edges of the illumination spot, and a broadening of the Fermi level (proportional to the charging) can be explained. In addition, the charged g/SiO_2 interface spot acts like an electrostatic lens on the emitted photoelectrons, thus decreasing the angular resolution of the photoemission data. The photo-induced charging therefore signifies a gating effect that we propose to be exploited in a device to measure ionizing radiation. Of course, for a detector application where the gate resistance is measured all other effects that affect the charge carrier concentration, such as the adsorption of gases [69] have to be considered.

5. Summary

It was shown that large, single-orientation graphene sheets grown on Ir(1 1 1) thin films may be transferred by help of a TOA-assisted wet chemistry method onto SiO_2 substrates. The resulting centimeter-sized structures with single-orientation graphene may be applied in devices using transport measurements, as well as for photoemission. The carrier density inferred from photoemission on an annealed sample in ultra high vacuum is, within the error bar, charge neutral, whereas the Dirac energy must be affected by the charging of the SiO_2 support that is directly determined from the same data.

Acknowledgments

The project got financial support from EU Horizon 2020 research and innovation program under grant agreement No. 696656 (GrapheneCore1-Graphene-based disruptive technologies) and the Swiss National Science Foundation SNF grant 200020_153312. Dr Wlodek Strupinski and

Dr Aleksandra Krajewska from the Institute of Electronic Materials Technology in Warsaw are gratefully acknowledged for introducing us to their electrochemical graphene transfer procedures. We thank Line Koefoed for fruitful exchange of information about the TOA-assisted delamination procedure and acknowledge Jean-Nicholas Longchamp for fruitful discussions. Anja Weber (Paul Scherrer Institut, Villigen) provided the SiO_2/Si substrates, and at the Center for Microscopy and Image Analysis of the University of Zurich the SEM measurements were performed.

ORCID iDs

B Probst https://orcid.org/0000-0001-8850-9685
G Mette https://orcid.org/0000-0001-7561-3264
T Greber https://orcid.org/0000-0002-8528-1969

References

[1] Novoselov K S, Jiang D, Schedin F, Booth T J, Khotkevich V V, Morozov S V and Geim A K 2005 *Proc. Natl Acad. Sci. USA* **102** 10451–3
[2] Bablich A, Kataria S and Lemme M C 2016 *Electronics* **5** 13
[3] Fiori G, Bonaccorso F, Iannaccone G, Palacios T, Neumaier D, Seabaugh A, Banerjee S K and Colombo L 2014 *Nat. Nanotechnol.* **9** 768
[4] Geim A K and Novoselov K S 2007 *Nat. Mater.* **6** 183
[5] Novoselov K S, Geim A K, Morozov S V, Jiang D, Zhang Y, Dubonos S V, Grigorieva I V and Firsov A A 2004 *Science* **306** 666–9
[6] Li X, Colombo L and Ruoff R S 2016 *Adv. Mater.* **28** 6247
[7] Banszerus L *et al* 2016 *Nano Lett.* **16** 1387–91
[8] Ohta T, Bostwick A, Seyller T, Horn K and Rotenberg E 2006 *Science* **313** 951
[9] Pletikosić I, Kralj M, Pervan P, Brako R, Coraux J, N'Diaye A T, Busse C and Michely T 2009 *Phys. Rev. Lett.* **102** 056808
[10] Brugger T, Günther S, Wang B, Dil J H, Bocquet M L, Osterwalder J, Wintterlin J and Greber T 2009 *Phys. Rev.* B **79** 045407
[11] Balog R *et al* 2010 *Nat. Mater.* **9** 315
[12] Larciprete R *et al* 2012 *ACS Nano* **6** 9551
[13] Knox K R, Locatelli A, Yilmaz M B, Cvetko D, Menteş T O, Nino M A, Kim P, Morgante A and Osgood R M 2011 *Phys. Rev.* B **84** 115401
[14] Knox K R, Wang S, Morgante A, Cvetko D, Locatelli A, Mentes T O, Nino M A, Kim P and Osgood R M 2008 *Phys. Rev.* B **78** 201408
[15] Hwang C, Siegel D, Mo S, Regan W, Ismach A, Zhang Y, Zettl A and Lanzara A 2012 *Sci. Rep.* **2** 590
[16] Kim K J *et al* 2008 *Adv. Mater.* **20** 3589
[17] Yan R *et al* 2012 *Appl. Phys. Lett.* **101** 022105
[18] N'Diaye A T, Coraux J, Plasa T N, Busse C and Michely T 2008 *New J. Phys.* **10** 043033
[19] Gsell S, Fischer M, Schreck M and Stritzker B 2009 *J. Cryst. Growth* **311** 3731–6
[20] Hemmi A *et al* 2014 *Rev. Sci. Instrum.* **85** 035101
[21] Wang Y, Zheng Y, Xu X, Dubuisson E, Bao Q, Lu J and Loh K P 2011 *ACS Nano* **5** 9927–33
[22] Gao L *et al* 2012 *Nat. Commun.* **3** 699
[23] Lupina G *et al* 2015 *ACS Nano* **9** 4776–85
[24] Šrut Rakić I, Čapeta D, Plodinec M and Kralj M 2016 *Carbon* **96** 243–9
[25] Koefoed L *et al* 2015 *J. Phys. D: Appl. Phys.* **48** 115306
[26] Zeller P, Dänhardt S, Gsell S, Schreck M and Wintterlin J 2012 *Surf. Sci.* **606** 1475–80
[27] Ciuk T, Pasternak I, Krajewska A, Sobieski J, Caban P, Szmidt J and Strupinski W 2013 *J. Phys. Chem.* C **117** 20833–7
[28] Truong Q T, Pokharel P, Song G S and Lee D S 2012 *J. Nanosci. Nanotechnol.* **12** 4305
[29] Bjerglund E, Kongsfelt M, Shimizu K, Jensen B B E, Koefoed L, Ceccato M, Skrydstrup T, Pedersen S U and Daasbjerg K 2014 *Langmuir* **30** 6622–8
[30] Simonet J and Lund H 1977 *J. Electroanal. Chem. Interfacial Electrochem.* **75** 719–30
[31] Greber T, Raetzo O, Kreutz T J, Schwaller P, Deichmann W, Wetli E and Osterwalder J 1997 *Rev. Sci. Instrum.* **68** 4549–54
[32] Cairns R B and Samson J A R 1966 *J. Opt. Soc. Am.* **56** 1568–73
[33] Jung I, Pelton M, Piner R, Dikin D A, Stankovich S, Watcharotone S, Hausner M and Ruoff R S 2007 *Nano Lett.* **7** 3569–75
[34] Ni Z H, Wang H M, Kasim J, Fan H M, Yu T, Wu Y H, Feng Y P and Shen Z X 2007 *Nano Lett.* **7** 2758–63
[35] Blake P, Hill E W, Castro Neto A H, Novoselov K S, Jiang D, Yang R, Booth T J and Geim A K 2007 *Appl. Phys. Lett.* **91** 063124
[36] Anders H 1967 *Thin Films in Optics* (London: Focal)
[37] Saito R, Hofmann M, Dresselhaus G, Jorio A and Dresselhaus M S 2011 *Adv. Phys.* **60** 413–550
[38] Ferrari A C and Basko D M 2013 *Nat. Nano* **8** 235
[39] Malard L, Pimenta M, Dresselhaus G and Dresselhaus M 2009 *Phys. Rep.* **473** 51–87
[40] Ferrari A C *et al* 2006 *Phys. Rev. Lett.* **97** 187401
[41] Ferrari A C 2007 *Solid State Commun.* **143** 47–57
[42] Hulman M, Haluška M, Scalia G, Obergfell D and Roth S 2008 *Nano Lett.* **8** 3594–97
[43] Haluška M *et al* 2007 *Phys. Status Solidi* b **244** 4143–6
[44] Pisana S, Lazzeri M, Casiraghi C, Novoselov K S, Geim A K, Ferrari A C and Mauri F 2007 *Nat. Mater.* **6** 198
[45] Yan J, Zhang Y, Kim P and Pinczuk A 2007 *Phys. Rev. Lett.* **98** 166802
[46] Ni Z, Wang Y, Yu T and Shen Z 2008 *Nano Res.* **1** 273–91
[47] Kim K, Coh S, Tan L Z, Regan W, Yuk J M, Chatterjee E, Crommie M F, Cohen M L, Louie S G and Zettl A 2012 *Phys. Rev. Lett.* **108** 246103
[48] Jorio A, Ferreira E M, Cancado L, Achete C and Capaz R 2011 Measuring disorder in graphene with raman spectroscopy *Physics and Applications of Graphene—Experiments* ed D S Mikhailov (Rijeka: InTech)
[49] Lillethorup M, Kongsfelt M, Ceccato M, Jensen B B E, Jorgensen B, Pedersen S U and Daasbjerg K 2014 *Small* **10** 922–34
[50] Lucchese M, Stavale F, Ferreira E M, Vilani C, Moutinho M, Capaz R B, Achete C and Jorio A 2010 *Carbon* **48** 1592–7
[51] Van Der Pauw L J 1958 *Philips Tech. Rev.* **20** 220–4
[52] Van Der Pauw L 1958 *Philips Res. Rep.* **13** 1–9
[53] Keywell F and Dorosheski G 1960 *Rev. Sci. Instrum.* **31** 833
[54] Du X, Skachko I, Barker A and Andrei E 2008 *Nat. Nanotechnol.* **3** 491
[55] Dean C *et al* 2010 *Nat. Nanotechnol.* **5** 722
[56] Bolotin K, Sikes K, Jiang Z, Klima M, Fudenberg G, Hone J, Kim P and Stormer H 2008 *Solid State Commun.* **146** 351
[57] Zhang Y, Brar V W, Girit C, Zettl A and Crommie M F 2009 *Nat. Phys.* **5** 722–6
[58] Samaddar S, Yudhistira I, Adam S, Courtois H and Winkelmann C B 2016 *Phys. Rev. Lett.* **116** 126804
[59] Martin J, Akerman N, Ulbricht G, Lohmann T, Smet J H, von Klitzing K and Yacoby A 2008 *Nat. Phys.* **4** 144–8
[60] Kröger J, Greber T, Kreutz T and Osterwalder J 2001 *J. Electron Spectrosc. Relat. Phenom.* **113** 241–51

[61] Wallace P R 1947 *Phys. Rev.* **71** 622–34
[62] Kundu R 2011 *Mod. Phys. Lett.* B **25** 163–73
[63] Bostwick A A, Ohta T, Seyller T, Horn K and Rotenberg E 2006 Experimental determination of the spectral function of graphene *Technical Report* No. cond-mat/0609660
[64] Reich S, Maultzsch J, Thomsen C and Ordejón P 2002 *Phys. Rev.* B **66** 035412
[65] Charlier J C, Gonze X and Michenaud J P 1991 *Phys. Rev.* B **43** 4579–89
[66] Malard L M, Nilsson J, Elias D C, Brant J C, Plentz F, Alves E S, Neto A H C and Pimenta M A 2007 *Phys. Rev.* B **76** 201401
[67] Kuzmenko A B, Crassee I, van der Marel D, Blake P and Novoselov K S 2009 *Phys. Rev.* B **80** 165406
[68] Nazin G, Zhang Y, Zhang L, Sutter E and Sutter P 2010 *Nat. Phys.* **6** 870
[69] Romero H E, Shen N, Joshi P, Gutierrez H R, Tadigadapa S A, Sofo J O and Eklund P C 2008 *ACS Nano* **2** 2037–44